American Mineralogist, Volume 85, pages 242–250, 2000

Kinoshitalite, $Ba(Mg)_3(Al_2Si_2)O_{10}(OH,F)_2$, a brittle mica from a manganese deposit in Oman: Paragenesis and crystal chemistry

EDWIN GNOS[1,*] AND THOMAS ARMBRUSTER[2]

[1]Mineralogisch-Petrographisches Institut, Baltzerstrasse 1, Universität Bern, CH-3012 Bern, Switzerland
[2]Laboratorium für Chemische und Mineralogische Kristallographie, Universität Bern, Freiestrasse 3, CH-3012 Bern, Switzerland

ABSTRACT

Kinoshitalite, ideally $Ba(Mg)_3(Al_2Si_2)O_{10}(OH,F)_2$, was studied in a granulite-facies manganese ore associated with calcium-bearing magnesian tephroite, hausmannite, calcite and manganoan clinochlore, and in a second assemblage together with hausmannite, altered tephroite, manganoan diopside, and calcite. The metamorphic rocks occur enclosed in peridotites of the Semail Ophiolite, Sultanate of Oman and were metamorphosed during ophiolite obduction.

Single-crystal X-ray data, collected on an inclusion-free kinoshitalite of $Ba_{0.99}K_{0.06}Na_{0.01}(Mg_{2.64}Mn_{0.31}Al_{2.01}Si_{2.03})O_{10}(OH_{1.61}F_{0.37}Cl_{0.02})$ composition, yielded a *C*-centered lattice of monoclinic symmetry with $a = 5.316(1)$, $b = 9.230(2)$, $c = 10.197(2)$ Å, $\beta = 100.06(1)°$, $V = 492.6$ Å^3, and $Z = 1$ characteristic of the 1 *M* polytype. The structure was refined in two models assuming complete Si, Al ordering in the space groups *C*2 and $C\bar{1}$ allowing for additional twinning. The data clearly suggest that in spite of the Si/Al ratio of 1 assumption of complete Si, Al ordering can be rejected. Two models, both in agreement with space group *C*2/*m*, causing Si, Al disorder, are discussed. Three-dimensional Si, Al disorder would lead to violation of the Al avoidance rule and substantial Ba displacement. The rather well defined Ba position capped by two six-membered rings of $Si_3Al_3O_{18}$ composition suggests one dimensional disorder where completely Si, Al ordered layers exist parallel to (001). The disorder occurs perpendicular to (001) and may be interpreted as random stacking faults.

INTRODUCTION

Kinoshitalite, $Ba(Mg)_3(Al_2Si_2)O_{10}(OH,F)_2$, belongs to the mica family (Guggenheim 1984) and was first reported by Yoshii et al. (1973a) as the Ba and Mg trioctahedral brittle mica. Natural barium-bearing micas occur in a variety of different rock types: igneous rocks (Thompson 1977; Wendlandt 1977; Mansker et al. 1979; Gaspar and Wyllie 1982; Edgar 1992; Bigi et al. 1993; Zhang et al. 1993), metasomatized rocks (Pan and Fleet 1991; Harlow 1995), marbles or calc-silicate rocks (Glassley 1975; Pattiaratchi et al. 1967; Rice 1977; Kretz 1980; Bucher-Nurminen 1982; Solie and Su 1987; Bol et al. 1989), and metamorphosed ore deposits (Frondel and Ito 1967; Yoshii et al. 1973a, Fleischer et al. 1975; Matsubara et al. 1976; Dasgupta et al. 1989; Tracy 1991; Chabu and Baulège 1992; Frimmel et al. 1995). Three end-member brittle mica minerals have the interlayer site completey occupied by Ba. Anandite, $Ba(Fe)_3(Fe^{3+}Si_3)O_{10}(OH)S$, is characterized by a trioctahedral sheet formed by Fe^{2+} octahedra, partial substitution of ferric iron in the tetrahedral layer, and unusual S^{2-} replacing OH^- or F^- (Pattiaratchi et al. 1967; Lovering and Widdowson 1968; Giuseppetti and Tadini 1972; Filut et al. 1985). In accord with the analyses published by Tracy (1991) and those of an unnamed Fe-analogue of kinoshitalite by Frimmel et al. (1995) there is also a mineral of $Ba(Fe)_3(Al_2Si_2)O_{10}(OH,Cl,F)_2$ composition which differs from anandite because the tetrahedral sheet is formed by Si and Al tetrahedra and it lacks S^{2-}. Except for the Mn-poor but Fe-bearing kinoshitalite from a high-grade metamorphic marble (Solie and Su 1987) all other known kinoshitalites are manganese-bearing or even manganoan and occur in amphibolite to granulite-facies metamorphosed manganese deposits (Yoshii et al. 1973a; Matsubara et al. 1976; Dasgupta et al. 1989), where barium is a common element of the protolith material (e.g., Kickmaier and Peters 1991).

Yoshii et al. (1973a) described the occurrence of kinoshitalite at Noda-Tamagawa mine in Japan where the mineral is associated with hausmannite and tephroite. In the same rock, but not in contact with kinoshitalite, occur celsian, quartz, spessartine, and rhodonite. In the Hokkejino occurrence described by Matsubara et al. (1976) the kinoshitalite is found in a banded manganese ore together with tephroite, manganoan diopside and sonolite, or associated with alabandite. The ore also contains in separate bands quartz and rhodonite, quartz and spessartine, and locally celsian, rhodochrosite and phlogopite. In the Precambrian Sausar Group of India (Dasgupta et al. 1989), kinoshitalite is closely associated with dolomite but also braunite, hausmannite, hematite, bixbyite, alkali feldspar, manganoan calcite, and quartz are described in the same sample.

Crystal structure refinements of kinoshitalite-1*M* by Kato et al. (1979), Guggenheim and Kato (1984), and Brigatti and

*E-mail: gnos@mpi.unibe.ch

0003-004X/00/0001–0242$05.00

Poppi (1993) found space group $C2/m$ leading to a disordered Si, Al distribution although the Si/Al ratio was close to 1. The composition of these samples strongly deviates from an end-member composition. Dasgupta et al. (1989) and Brigatti and Poppi (1993) described an apparent continuous chemical series between trioctahedral phlogopite and trioctahedral kinoshitalite. Yoshii et al. (1973b) showed that the exchange vectors operating are K + Si ↔ Ba + Al, and independent from this Mn ↔ Mg. Yoshii and Maeda (1975) also investigated the relations between barium content and optical properties of micas along this join and concluded that the birefringence decreases with increasing Ba content parallel to an increase of the a cell dimension, and that the transition from the phlogopite to the kinoshitalite structure occurs near Ba:K = 1:2. This observation points to a discontinuous join also confirmed by the structural studies of Brigatti and Poppi (1993).

Kinoshitalite end-members were synthesized by Hatch et al. (1957) from melts of appropriate composition by cooling at a rate of 2° per minute through the crystallization range and by Frondel and Ito (1967) by heating gels in water in a cold-seal steal vessel at 650 °C and 0.2 GPa for 48 hours. Hatch et al. (1957) noted that synthetic $BaMg_3(Al_2Si_2)O_{10}(F)_2$ could not be formed below 1000 °C at a pressure of 1 bar. Hatch et al. (1957) and Bloss et al. (1959) noted a significant increase in mica hardness with higher Ba content.

The discovery of close to end-member natural kinoshitalite of good crystal quality in a manganese deposit located in the Oman mountains motivated us to study this unusual occurrence and to re-examine the crystal structure for possible Si, Al ordering.

Geologic setting

The kinoshitalite-bearing samples are from granulite-facies metamorphic manganese ore which occurs associated with marbles, calcsilicate rocks, amphibolites and quartzo-feldspatic rocks in a sequence enclosed in peridotites of the Semail Ophiolite, Oman (Fig. 1). The granulite-facies rocks formed during the thrusting of the Semail Ophiolite onto the Arabian continental edge in the Late Cretaceous (e.g., Reinhardt 1969;

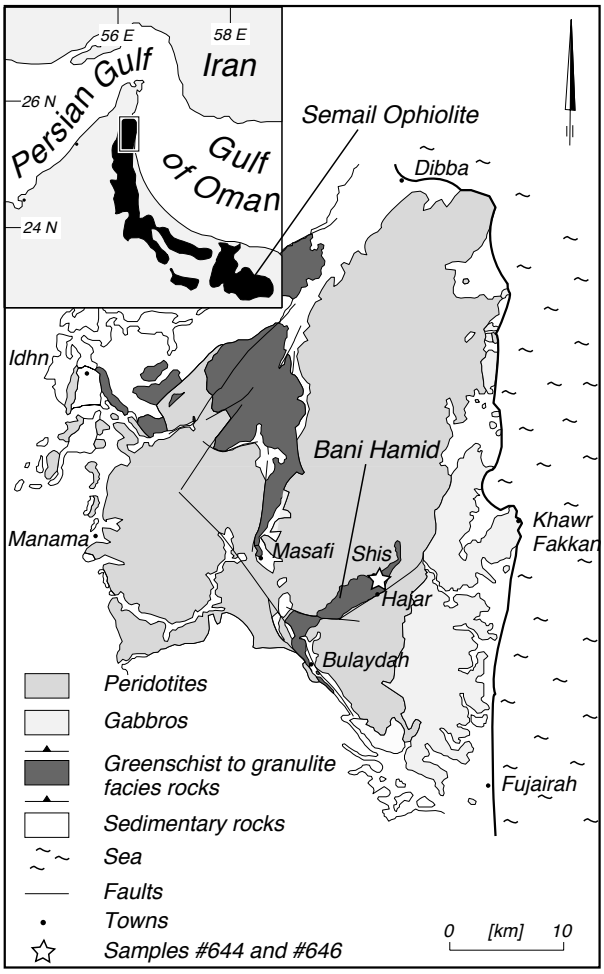

Figure 1. Geologic setting of the granulite-facies metamorphic rocks (Bani Hamid unit) enclosed in peridotite near the northern termination of the Semail Ophiolite, Sultanate of Oman and United Arab Emirates. The location of the kinoshitalite-bearing rocks on the west side of the gorge to Hajar village is marked by a star.

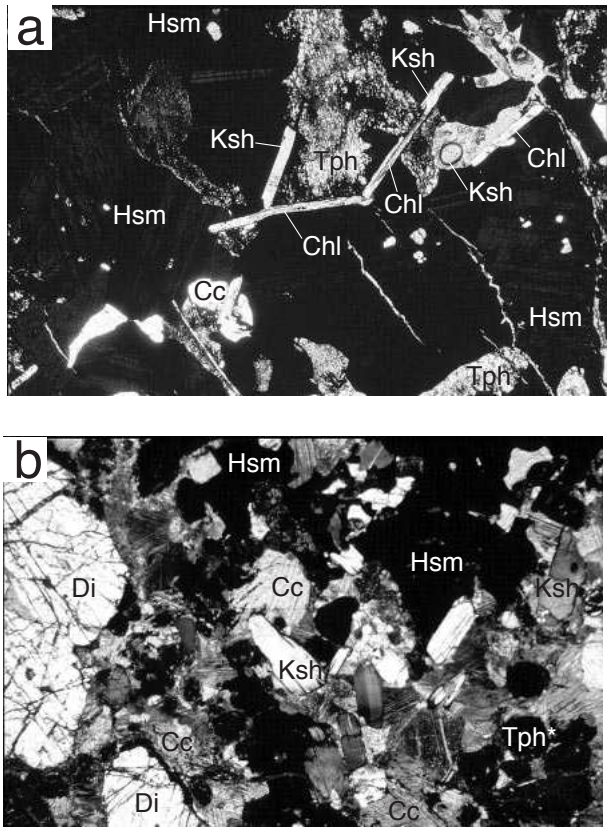

Figure 2. Photomicrographs of kinoshitalite-bearing samples. Base of picture = 4.5 mm. (**a**) Sample no. 644, crossed polars. (**b**) Sample no. 646, crossed polars. Ksh = kinoshitalite; Hsm = Hausmannite; Tph = tephroite; Tph* = pseudomorps after tephroite or Mn-humite; Di = manganoan diopside; Cc = calcite. In no. 644 manganoan clinochlore and kinoshitalite are closely associated and optically hardly distinguishable.

TABLE 1. Microprobe analyses of kinoshitalite

Sample	644 ksh11	644 ksh3	644 ksh6	644 ksh9	644* ksh15	644* ksh30	646 ksh8	646 ksh9	646 ksh36	646 ksh40	646 ksh42
SiO_2	22.94	22.92	23.52	23.42	23.07(41)	22.91(24)	29.44	28.77	26.95	28.55	28.22
TiO_2	0.00	0.06	0.12	0.09	0.05(4)	0.04(4)	0.51	0.39	0.77	0.41	0.38
Cr_2O_3	0.00	0.00	0.00	0.00	0.00(0)	0.00(0)	0.00	0.00	0.00	0.00	0.07
Al_2O_3	19.58	19.52	19.23	19.34	19.35(8)	19.53(7)	17.16	17.35	17.21	17.32	17.47
Fe_2O_3	0.04	0.00	0.02	0.01	0.02(3)	0.03(2)	0.40	0.31	0.68	0.22	0.24
MnO	4.41	4.32	3.98	4.14	4.20(25)	4.28(17)	3.01	3.11	2.76	3.13	3.14
MgO	19.80	19.87	20.30	20.24	20.09(24)	19.84(19)	21.96	22.07	21.83	22.30	22.15
CaO	0.00	0.01	0.00	0.01	0.00(1)	0.00(0)	0.04	0.03	0.01	0.01	0.01
Na_2O	0.04	0.03	0.07	0.05	0.06(1)	0.05(1)	0.13	0.14	0.12	0.14	0.15
K_2O	0.11	0.15	0.79	0.73	0.53(20)	0.16(7)	3.07	3.12	2.51	3.32	3.29
BaO	28.91	29.25	27.90	28.37	28.61(58)	29.12(80)	20.35	20.77	23.09	20.71	20.43
F	1.39	1.46	1.35	1.21	1.32(8)	1.46(6)	1.22	0.99	1.04	1.24	1.11
Cl	0.12	0.16	0.09	0.13	0.12(2)	0.14(2)	0.03	0.04	0.04	0.04	0.03
H_2O*	2.71	2.66	2.76	2.82	2.74(5)	2.66(4)	3.10	3.19	3.08	3.07	3.11
Total	100.05	100.41	101.13	100.56	100.16(56)	100.22(42)	100.42	100.28	100.09	100.46	99.80
Si	2.025	2.023	2.058	2.049	2.032(22)	2.025(11)	2.395	2.354	2.252	2.334	2.316
Al^{IV}	1.975	1.977	1.942	1.951	1.968(22)	1.975(11)	1.605	1.646	1.695	1.666	1.684
Sum	4.000	4.000	4.000	4.000	4.000(0)	4.000(0)	4.000	4.000	3.947	4.000	4.000
Ti	0.000	0.004	0.008	0.006	0.003(3)	0.003(3)	0.032	0.024	0.048	0.025	0.023
Cr	0.000	0.000	0.000	0.000	0.000(0)	0.000(0)	0.000	0.000	0.000	0.000	0.004
Al^{VI}	0.062	0.054	0.042	0.043	0.041(9)	0.059(8)	0.041	0.027	0.000	0.003	0.006
Fe^{3+}	0.002	0.000	0.001	0.001	0.002(2)	0.002(1)	0.024	0.019	0.043	0.014	0.015
Mn	0.330	0.323	0.295	0.307	0.314(21)	0.321(12)	0.208	0.216	0.195	0.217	0.218
Mg	2.606	2.615	2.647	2.639	2.638(15)	2.614(12)	2.664	2.691	2.718	2.717	2.710
Sum	3.000	2.996	2.993	2.996	2.998(3)	2.999(3)	2.969	2.977	3.004	2.976	2.976
Ca	0.000	0.001	0.000	0.001	0.000(1)	0.000(0)	0.003	0.003	0.000	0.001	0.001
Na	0.007	0.005	0.011	0.008	0.010(2)	0.009(2)	0.020	0.022	0.020	0.022	0.024
K	0.012	0.017	0.089	0.081	0.060(23)	0.019(7)	0.319	0.326	0.267	0.346	0.344
Ba	1.000	1.012	0.957	0.972	0.988(25)	1.008(33)	0.649	0.666	0.754	0.663	0.657
Sum	1.019	1.035	1.057	1.062	1.036(28)	1.058(16)	0.991	1.017	1.041	1.032	1.026
F	0.338	0.408	0.372	0.336	0.369(23)	0.407(18)	0.313	0.255	0.274	0.321	0.289
Cl	0.018	0.024	0.014	0.019	0.018(3)	0.021(2)	0.004	0.005	0.006	0.006	0.005
OH	1.644	1.568	1.614	1.645	1.613(23)	1.572(18)	1.683	1.740	1.720	1.673	1.706
Sum	2.000	2.000	2.000	2.000	2.000(0)	2.000(0)	2.000	2.000	2.000	2.000	2.000

Note: Oxides are given in weight percent.
* H_2O is calculated by stoichiometry. Normalization based on 7 cations (total cations-Ca-Na-K-Ba = 7-Ti), and 24 negative charges; Average of 15 analyses with standard deviation.

Allemann and Peters 1972; Glennie et al. 1974). Accreted material adjacent to the hot peridotite hanging wall was metamorphosed during ophiolite thrusting. Near the northern end of the Semail ophiolite, sedimentary and igneous rocks were during thrusting tectonically enclosed in the peridotites of the mantle sequence and metamorphosed by the hot peridotite to granulite-facies conditions (Gnos and Kurz 1994; Gnos and Nicolas 1996). Metamorphic equilibration conditions were estimated at 0.65–0.9 GPa and 800 ± 50° C (Gnos and Kurz 1994), and peak metamorphic temperatures may have been higher (Gnos and Nicolas 1996). Associated quartz-rich lithologies contain two-pyroxene-magnetite/titanian hematite, magnetite-spinel-titanohematite-enstatite-(±sapphirine), magnetite-titanian hematite-enstatite-(±sillimanite), and amphibolites contain clinopyroxene or clinopyroxene-orthopyroxene (Gnos and Kurz 1994). Most of the manganese ore occurs associated with quartzites, less often it is associated with meta-carbonates or amphibolites (Gnos et al. 1996; Gnos and Peters 1995). Our kinoshitalite-bearing samples are from up to 10 cm thick boudinaged and folded Mn-ore layers associated with meta-carbonates and located on the west side of the gorge that leads to Shis village and crosses the metamorphic sequence (Fig. 1).

SAMPLE DESCRIPTION

Kinoshitalite plates up to 3 mm in diameter were observed in two hand specimens (no. 644 and no. 646) consisting of medium-grained, black hausmannite ore with patches of carbonate or grayish pyroxene. The Ba brittle mica can macroscopically not be distinguished from phlogopite which is a common mineral in associated metamorphic enstatite or cordiertite quartzites (Gnos and Kurz 1994). In thin section no. 644 kinoshitalite, manganoan tephroite and calcite occur randomly distributed in a matrix of red transparent hausmannite displaying twinning lamellae (Fig. 2a). Kinoshitalite shows no to very weak pleochroism, is colorless to slightly yellowish and commonly associated or intergrown with manganoan chlorite (Fig. 2a). Albite and manganoan diopside occur in trace amounts. Tephroite shows partial alteration to serpentine-group minerals. In sample no. 646, ~5 vol% of the rock is kinoshitalite that occurs concentrated in a folded band and in textural equilibrium with calcite, hausmannite, altered tephroite, manganoan diopside, and in the tephroite-free part with minor quartz (Fig. 2b). Kinoshitalite in this sample is generally light yellow and weakly pleochroitic.

MINERAL CHEMISTRY

Minerals were analyzed on a Cameca SX-50 microprobe using beam conditions of 15 kV and 20 nA, wavelength-dispersive spectrometers, and an enlarged spot size of ~10 μm to minimize damage of hydrous minerals. Natural and synthetic minerals were used as standards. Ti$K\alpha$ and Ba$L\alpha$ were measured on a LiF crystal where the two lines are not overlapping.

Benitoite was used as Ba standard, synthetic fluor phlogopite for fluorine and scapolite for chlorine. Data for Ba, Ti, F, and Cl were collected for 30 s, all other elements for 20 s.

Due to the Fe-poor bulk rock composition all minerals in sample no. 644 are Fe-free. In sample no. 646 iron is only present in kinoshitalite and is assumed to be ferric.

Most analyses of kinoshitalite in sample no. 644 are nearly K-free and have a composition near $Ba_{1.00}(Mg_{2.7}Mn_{0.3})(Al_2Si_2)O_{10}(OH_{1.6}F_{0.4})$ (Table 1) with only traces of K, Ca, and Cl. In a mica concentrate of sample no. 644, many grains show intergrowth with hausmannite or manganoan clinochlore. From this concentrate a yellowish but clear crystal of composition $Ba_{0.99}K_{0.06}Na_{0.01}(Mg_{2.64}Mn_{0.31}Al_{2.01}Si_{2.03})O_{10}(OH_{1.61}F_{0.37}Cl_{0.02})$ (Table 1, 644ksh15) was used for the single-crystal structural refinement. A second, colorless crystal of composition $(Ba_{1.01}K_{0.02}Na_{0.01})(Mg_{2.61}Mn_{0.32}Al_{2.03}Si_{2.03})O_{10}(OH_{1.57}F_{0.41}Cl_{0.02})$ (Table 1, 644ksh30) was used for determination of the cell parameters by single-crystal X-ray methods yielding $a = 5.331(1)$, $b = 9.240(2)$, $c = 10.214(3)$ Å, $\beta = 100.09(2)°$. In sample no. 646 Ba in kinoshitalite is partially replaced by K. The composition is homogeneous throughout the sample (Table 1), with an average of $(Ba_{0.70}K_{0.31})(Mg_{2.71}Mn_{0.21}Fe^{3+}_{0.03})(Al_{1.68}Si_{2.31})O_{10}(F_{0.29}OH_{1.70}Cl_{0.01})$. In comparison with sample no. 644 the small amounts of ferric iron seem sufficient to give the mica a more pronounced yellowish color in thin section and a macroscopic appearance like phlogopite.

Tephroite in sample no. 644, which comprises ~15–20% of the rock, is Fe-free, rich in Mg, and has the composition $(Mn_{1.18}Mg_{0.69}Ca_{0.14})SiO_4$ (Table 2, 644tph1). Such a composition is often referred to as "picrotephroite" (Deer et al. 1982). Compared with published "picrotephroite" analyses, our material is rich in Ca. The tephroite shows alteration to serpentine-like minerals. A representative microprobe analysis of tephroite is listed in Table 2. Tephroite or a Mn-humite mineral was also present in the calcite-rich part in sample no. 646. It is completely replaced by very fine-grained black, non-transparent material. Qualitative analyses indicate that this material consists probably mainly of a mixture of caryopilite (serpentine-like Mn-rich mineral) and chrysotile.

Manganoan diopside is a major constituent of sample no. 646, forming approximately 30% of the rock. The chemical variation is very small and the average composition is $(Mn_{0.13}Mg_{0.97}Ca_{0.91})(Si_{2.00})O_6$ (Table 2). A few diopside grains occur also in sample no. 644 with a composition of $(Mn_{0.19}Mg_{0.88}Ca_{0.96})(Si_{1.96}Al_{0.02})O_6$ (Table 2).

In sample no. 644 hausmannite is with 60–70% the main constituent. It has a homogeneous composition close to end-member with traces of Mg and Al (Table 2). In sample no. 646 hausmannite forms ~40% of the rock. The composition is similar to sample no. 644, with slightly higher Mg contents (Table 2).

In both samples calcite grains exhibit characteristic deformation twins. Although they occur in contact with Mn-rich minerals the MnO contents are generally below 3 wt% (Table 2). BaO contents are typically 1–2 wt% and Sr was not found in measurable quantities. In sample no. 646 calcite grains in contact with hausmannite show higher manganese contents of up to 9.5 wt% MnO (Table 2).

In sample no. 644 manganoan clinochlore occurs in close association or even intergrown with kinoshitalite and appears to be stable under granulite-facies conditions. This clinochlore is Fe-free with an average composition of $(Mn_{0.47}Mg_{4.41}Al_{1.08})(Si_{2.99}Al_{1.01})O_{10}(OH)_8$ (Table 2).

TABLE 2. Minerals coexisting with kinoshitalite

Sample	644 chl4	644 hsm34	644 di36	644 tph1	644 cc46	646 di1	646 hsm1	646 cc10	646 cc16
SiO_2	30.87	0.02	53.83	33.39	0.04	55.15	0.00	0.08	0.04
TiO_2	0.00	0.05	0.03	0.00	0.00	0.09	0.09	0.00	0.06
Cr_2O_3	0.00	0.05	0.00	0.00	0.00	0.04	0.05	0.03	0.00
Al_2O_3	18.32	0.48	0.44	0.01	0.00	0.19	0.21	0.02	0.01
FeO	0.00	0.00	0.00	0.00	0.05	0.00	0.00	0.00	0.00
MnO	5.76	91.58	6.07	46.69	0.39	3.77	91.49	9.41	2.72
MgO	30.52	0.51	16.15	15.46	0.09	17.83	0.71	0.60	0.76
BaO	—	—	—	—	0.74	—	—	2.00	0.93
CaO	0.03	0.05	24.58	4.48	52.23	23.16	0.00	41.52	50.42
Na_2O	0.01	0.00	0.00	0.02	0.02	0.03	0.02	0.03	0.01
K_2O	0.02	0.00	0.00	0.00	0.00	0.01	0.00	0.00	0.01
F	0.10	—	—	—	0.00	—	—	0.00	0.00
Cl	0.02	—	—	—	0.03	—	—	0.07	0.01
Total	85.65	92.74	101.10	100.05	53.59	100.27	92.57	53.76	54.97
	(*)	(†)	(‡)	(§)	(ll)	(‡)	(†)	(ll)	(ll)
Si	2.993	0.001	1.959	0.993	0.001	2.003	0.000	0.003	0.001
Ti	0.000	0.002	0.001	0.000	0.000	0.002	0.003	0.000	0.002
Cr	0.000	0.002	0.000	0.000	0.000	0.001	0.001	0.001	0.000
Al	2.094	0.022	0.019	0.001	0.000	0.008	0.009	0.001	0.000
Fe	0.000	0.000	0.000	0.000	0.001	0.000	0.000	0.000	0.000
Mn	0.473	2.944	0.187	1.177	0.012	0.116	2.945	0.293	0.080
Mg	4.412	0.029	0.876	0.686	0.005	0.965	0.040	0.033	0.039
Ba	—	—	—	—	0.010	—	—	0.029	0.013
Ca	0.003	0.002	0.959	0.143	1.969	0.901	0.000	1.638	1.864
Na	0.002	0.000	0.000	0.001	0.001	0.002	0.002	0.002	0.001
K	0.002	0.000	0.000	0.000	0.000	0.001	0.000	0.000	0.000
F	0.031	—	—	—	0.000	—	—	0.000	0.000
Cl	0.003	—	—	—	0.002	—	—	0.004	0.001

Note: Analyses are normalized to: (*) 140; (†) 40 and 3 cations; (‡) 60 and 4 cations; (§) 40 and 3 cations; (ll) 2 cations.

SINGLE-CRYSTAL X-RAY DATA COLLECTION AND REFINEMENT

A yellow-brown flaky crystal ($0.3 \times 0.3 \times 0.05$ mm^3) without microscopic inclusions was selected for structural study with an ENRAF NONIUS CAD4 single-crystal X-ray diffractometer using graphite monochromated Mo$K\alpha$ X-radiation at room temperature (293 K). Cell dimensions were refined from the angular settings of 24 reflections with $12 < \theta < 24°$ yielding monoclinic symmetry with a = 5.316(1), b = 9.230(2), c = 10.197(2) Å, β = 100.06(1)°. The crystal of $Ba_{0.99}K_{0.06}Na_{0.01}(Mg_{2.64}Mn_{0.31}Al_{2.01}Si_{2.03})O_{10}$ $(OH_{1.61}F_{0.37}Cl_{0.02})$ composition (Table 1, 644ksh15) did not show any indication of twinning in its X-ray diffraction pattern.

Diffraction data were collected up to $\theta = 40°$ (a full sphere of the reciprocal space up to $\theta = 25°$; and one quadrant between 25 and 40°). Experimental details are in Table 3. Data reduction, including background and Lorenz polarization correction, was carried out with the SDP program system (Enraf-Nonius 1983). An empirical absorption correction using the ψ-scan technique was applied. An analytical absorption correction was also tested but the empirical model was found superior based on R_{int} of symmetry equivalent reflections. Structure solution and refinement were performed with neutral atom scattering factors and the programs SHELXS-97 and SHELXL-97 (Sheldrick 1997). The structure was refined in various models: (1) space group $C2$, allowing for twinning $\bar{h}\,\bar{k}\,\bar{l}$; (2) space group $C\bar{1}$, allowing for twinning $h\,\bar{k}\,l$, or $\bar{h}\,k\,\bar{l}$; and (3) disordered in space group $C2/m$. Because low-angle data are more sensitive for the localization of H positions than high angle data, the full-sphere data set (up to $\theta = 25°$) was used to extract the H site from the difference-Fourier map. The corresponding electron density peak of 0.6 e/Å^3 was the strongest peak in the map and could therefore unambigupously be assigned. All positions (except H) were refined with anisotropic displacement parameters. According to the electron microprobe analyses the Mg, Mn occupancies of the octahedral sites were allowed to vary. In final least square cycles the H4 site was constrained to be 1.00(5) Å apart from the neighboring O4 position. Thus O4 and H4 form a regular OH group. The atom-labeling scheme was adopted from Guggenheim and Kato (1984). In space group $C2/m$ there is only one symmetry independent tetrahedral site and mixed Si, Al scattering curves must be assigned. Atomic coordinates and displacement parameters are in Tables 4 and 5. Selected interatomic distances are in Table 6.

TABLE 3. Data collection and refinement parameters of kinoshitalite

Crystal size (mm^3)	$0.30 \times 0.30 \times 0.05$
Diffractometer	Enraf Nonius CAD4
X-ray radiation	sealed tube Mo$K\alpha$, graphite monochromaticed
X-ray power	55 kV, 40 mA
Temperature	293 K
Reflections measured	2791
Max. θ	40°
h, k, l limits	$-9 \le h \le 9$, $-10 \le k \le 16$, $-12 \le l \le 18$
Unique reflections > 3σ(I)	1492
Space group	$C2/m$ (no. 12)
cell dimensions (Å)	
Angle	a = 5.316(1) b = 9.230(2), c = 10.197(2), β = 100.06(1)°
R(int) after empirical absorption correction	1.91%
R(σ)	1.43%
Number of l.s. parameters	60
GoF	1.012
R1, $F_o > 4\sigma(F_o)$	3.35%
wR2 (on F^2)	8.83%

Note: $R1 = \left(\Sigma\|F_o|-|F_c\|\right)/\left(\Sigma|F_o|\right)$ $\quad wR2 = \sqrt{\left[\Sigma\left(F_o^2 - F_o^2\right)^2\right]/\left[\Sigma w\left(F_o^2\right)^2\right]}$

$GoF = \sqrt{\left[\Sigma w\left(F_o^2 - F_c^2\right)^2\right]/(n-p)}$

CRYSTAL STRUCTURE

*C*2 model

The hypothetical $C2$ polytype of kinoshitalite-1M is characterized by completely Si, Al ordered tetrahedral layers with two symmetry independent T sites, one occupied by Al, the other by Si. Each Si tetrahedron is adjacent to three Al tetrahedra and vice versa (Fig. 3), preserving Loewenstein's (1954) Al avoidance rule. The tetrahedral sheets are arranged above and below the Ba level such that along the c-axis Si is always adjacent to Si. Correspondingly, Al is adjacent to Al. Three symmetry independent octahedral sites exist in this space group. Refinement in this model led to identical T-O distances for both T sites which were highly correlated. In addition, the three octahedral positions converged to identical Mg, Mn populations. Introduction of bond length constraints forcing one T site to have longer T-O distances (~1.76 Å) characteristic of Al and the other to have short T-O distances (~1.62 Å) characteristic of Si led to a significant increase of the R-values. When the bond-lengths constraints were released, T-O distances converged to more even values. Thus the $C2$ model can be rejected.

TABLE 4. Atomic coordinates, populations, and B_{eq} for kinoshitaite

site	occupancy	x/a	y/b	z/c	B_{eq} (Å^2)
I	0.94 Ba 0.06 K	1/2	1/2	1/2	1.521(4)
M1	0.92(1) Mg 0.08(1) Mn	0	1/2	0	0.84(2)
M2	0.912(6) Mg 0.088(6) Mn	0	0.16937(9)	0	0.88(1)
T	0.5 Si 0.5 Al	0.0750(1)	0.33339(6)	–0.27599(5)	0.903(7)
O1		0.0081(5)	1/2	0.3395(2)	1.49(3)
O2		0.1656(3)	0.2193(2)	0.3393(2)	1.49(2)
O3		0.1302(3)	0.3337(2)	–0.1106(1)	1.16(2)
O4		0.1315(4)	0	–0.1025(2)	1.14(2)
H4		0.09(1)	0	–0.192(4)	2.2(12)

TABLE 5. Anisotropic atomic displacement parameters for kinoshitalite

site	U_{11}	U_{22}	U_{33}	U_{12}	U_{13}	U_{23}
I	0.0210(1)	0.0190(1)	0.0179(1)	0	0.00359(7)	0
M1	0.0113(5)	0.0091(5)	0.0118(5) 0	0.0026(3)	0	0
M2	0.0117(4)	0.0097(4)	0.0120(4)	0	0.0021(2)	0
T	0.0125(2)	0.0103(2)	0.0117(2)	–0.0002(1)	0.0026(1)	0.0002(1)
O1	0.0243(9)	0.0148(8)	0.0156(8)	0	–0.0017(6)	0
O2	0.0197(6)	0.0216(6)	0.0161(5)	0.0050(5)	0.0056(4)	0.0040(4)
O3	0.0147(5)	0.0123(5)	0.0172(5)	–0.0006(4)	0.0036(4)	0.0003(4)
O4	0.0143(7)	0.0149(7)	0.0142(7)	0	0.0023(5)	0

TABLE 6. Selected interatomic distances (Å) and angles (°) for kinoshitalite

I-O1 ×2	2.832(2)	T-O3	1.660(2)
I-O2 ×4	2.839(2)	T-O2	1.693(2)
mean	2.837	T-O2	1.695(2)
I-O1' ×2	3.394(3)	T-O1	1.697(1)
I-O2' ×4	3.397(2)	mean	1.686
mean	3.396		
		T-O1-T	130.0(1)
M1-O4 ×2	2.053(2)	T-O2-T	130.1(1)
M1-O3 ×4	2.093(1)		
mean	2.080	O4-H4	0.90(4)
		H4-O2 ×2	2.74(3)
M2-O4 ×2	2.069(1)	H4-O1	2.81(6)
M2-O3 ×2	2.079(1)	O4-O1	3.330(2)
M2-O3 ×2	2.089(1)	O4-O2 ×2	3.336(3)
mean	2.079		

$C\bar{1}$ model

The hypothetical $C\bar{1}$ polytype of kinoshitalite is also characterized by complete Si, Al ordering within the tetrahedral sheets. The difference between the $C\bar{1}$ and C2 models can be seen if adjacent layers above and below the Ba level are compared (Fig. 4). Above or below parallel to the *c* axis, an Si tetrahedron is always adjacent to an Al tetrahedron and vice versa. This model has only two symmetry independent octahedral sites. Refinement in this model led to identical T-O distances for both T sites which were again highly correlated. Introduction of bond length constraints, forcing one T site to have longer T-O distances (~1.76 Å) characteristic of Al and the other to have short T-O distances (~1.62 Å), led to a significant increase of the *R*-values. As in the *C*2 model, release of bond-lengths constraints led to more even T-O distances. Thus the $C\bar{1}$ model can also be rejected.

$C\bar{1}$ and *C*2 twin models

Twinning in space group $C\bar{1}$ was tested for $\bar{h}\ k\ \bar{l}$ and $h\ \bar{k}\ l$ reflection transformations. In space group *C*2 twinning by the center of symmetry ($\bar{h}\ \bar{k}\ \bar{l}$) was tested. These types of twinning mean that large coherent blocks of one of the hypothetical polytypes exist, the orientation of which is transformed by a twin operation. Applying these twin models on F^2 and allowing the population of the two different twin individuals to be refined yielded in each case a 1:1 twin ratio but a distinction between large Al and small Si tetrahedral sites could not be made. Positions related by pseudo-symmetry exhibited correlation coefficients greater 0.9. Furthermore, introduction of tetrahedral bond lengths constraints (see above) led to an increase of the R-value, thus the hypothesis of twinning parallel to (001) of completely Si, Al ordered polytypes can be rejected.

*C*2/*m* disorder model

Two models must be distinguished: (1) three-dimensional Si, Al disorder. This model implies the violation of the Al avoidance rule within a tetrahedral layer. Thus there are locally adjacent Al tetrahedra and correspondingly adjacent Si tetrahedra. (2) One dimensional disorder, where the individual layers are completely Si, Al ordered, is in agreement with the Al avoidance rule. This disorder occurs in the stacking direction parallel to *c*. Thus, there is a random stacking of layers where either two chemically identical or two chemically different tetrahedra are adjacent parallel to *c*. Based on the X-ray diffraction behavior both disorder models lead to average *C*2/*m* symmetry and cannot be distinguished. Reflection intensities measured for kinoshitalite are in agreement with both disorder models and corresponding average coordinates are given in Table 4. In particular, the *C*2/*m* model yields good agreement between F_{obs} and F_{calc} for weak reflections which are especially sensitive for wrong space-group assignments. In *C*2/*m* there are two symmetry independent octahedral sites which are both occupied by 91% Mg and 9% Mn, which is in good agreement with the electron microprobe analyses performed on the same crystal.

DISCUSSION

Comparison with previous studies

The possibility of tetrahedral Si, Al ordering in kinoshitalite was addressed by Kato et al. (1979) and Guggenheim and Kato (1984). The latter authors also determined space group *C*2/*m* for a kinoshitalite-1*M* leading to Si, Al disorder but they could not rule out that their crystals were twinned. Furthermore, their crystals and those studied by Brigatti and Poppi (1993) had a much more complex chemical composition than the close to end-member crystal investigated here. One of the major chemical differences between the kinoshitalites previously refined and our sample is the Ba concentration on the interlayer site I. In the previous studies, the Ba concentration on the interlayer site I was below 54% with additional K and Na, whereas in kinoshitalite from Oman the Ba concentration on I is close to 100%. Furthermore, in the previous studies additional three valent elements (mainly Al with minor Mn^{3+}) were found on the octahedral M sites balancing substitution of K and Na for Ba on I. As a consequence, the present sample has significantly smaller cell dimensions (*a*, *b*, and *c*) which is mainly reflected in shortened I-O distances where the I site has six short I-O distances of average 2.837 Å with additional six long I-O bonds of 3.4 Å. In kinoshitalite with only 54% Ba on I (crystal no. 6 of Kato et al. 1979) the corresponding short distance is 2.866 Å. Thus Ba on I strongly strengthens the interlayer bonds. For

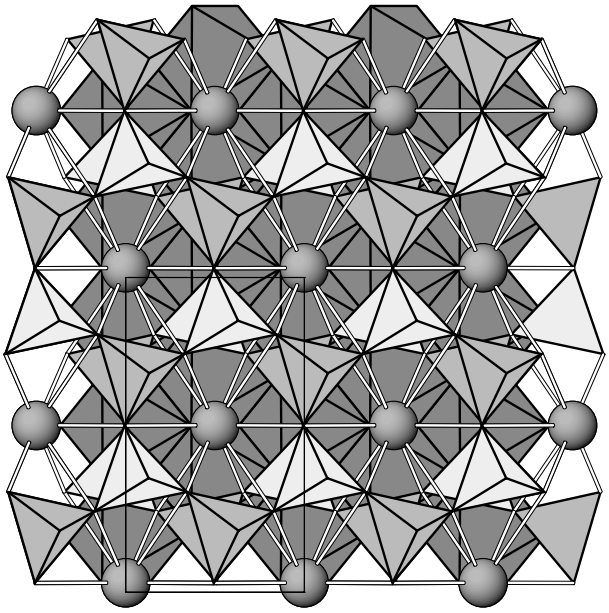

FIGURE 3. Polyhedral model of the hypothetical kinoshitalite-1*M* polytype with space group *C*2, projected on (001). Si tetrahedra are light and Al tetrahedra are dark, respectively. Notice that the tetrahedral layers are completely Si, Al ordered. Parallel to the *c* axis, Si tetrahedra are adjacent to Si, and Al tetrahedra are adjacent to Al. Open lines represent bonds between Ba (spheres) and the twelve closest oxygen positions. Thin black lines border the unit cell.

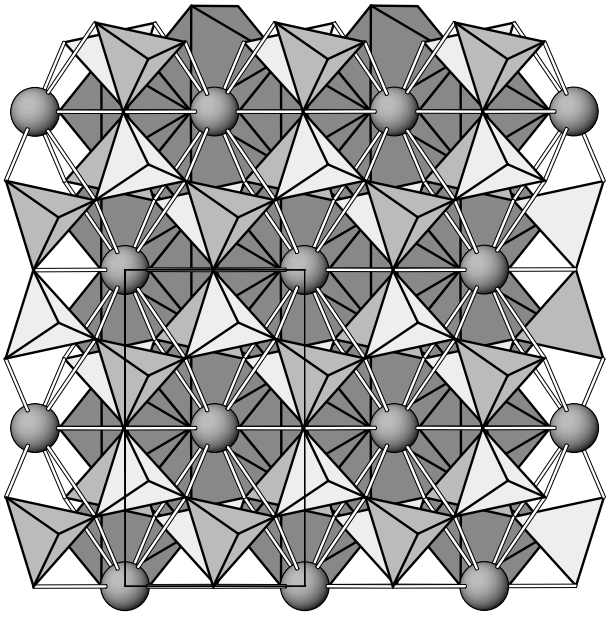

FIGURE 4. Polyhedral model of the hypothetical kinoshitalite-1*M* polytype with space group $C\bar{1}$, projected on (001). Si tetrahedra are light and Al tetrahedra are dark. Notice that the tetrahedral layers are completely Si, Al ordered. Parallel to the *c* axis, Si tetrahedra are adjacent to Al tetrahedra and vice versa. Open lines represent bonds between Ba (spheres) and the twelve closest oxygen positions. Thin black lines border the unit cell.

comparison, K in biotite-1*M* has 12 I-O distances between 3.00 and 3.35 Å (Brigatti and Davoli 1990).

Due to the higher Ba population the tetrahedral rotation angle ($\alpha = 17.89°$) for Oman kinoshitalite is considerably larger than the maximum value of 12.6° given by Kato et al. (1979) for their alkali-rich kinoshitalite. The strong trigonal deformation of the tetrahedral rings in kinoshitalite-1*M* is in contrast to the almost ideal hexagonal ring topology observed for anandite, $Ba(Fe^{2+})_3(Si_{2.6}Fe^{3+}_{1.4})O_{10}(OH)S$, with $\alpha = 0.09°$ (Filut et al. 1985). The octahedral thickness t_o in Oman kinoshitalite is 2.167 Å leading to octahedral ψ of 58.6° (Bailey 1984). The tetrahedral thickness t_t is 2.297 Å, and the interlayer distance is 3.225 Å.

Si, Al order-disorder

Modern crystal-structure refinement techniques allow refinement of various twin models which were tested in the present study. If in the twin models of space group $C\bar{1}$ or *C*2 the tetrahedral dimensions are constrained to fulfill complete Si, Al ordering, then the atomic displacement parameters do not decrease compared to the average *C*2/*m* model. This is an additional indication that the lower space groups (even with additional twinning assumed) do not lead to an acceptable model for kinoshitalite. Kunz and Armbruster (1990) modeled the effect of Si, Al disorder on difference atomic displacement parameters (ΔU) evaluated along the T-O bonding vector in alkali feldspars. They found that ΔU for a pure SiO_4 and AlO_4 tetrahedron is 0.0004 Å^2 and 0.0005 Å^2, respectively. In case of 1:1 disorder of Si and Al in a tetrahedron, the T-O bond distance difference of approximately 0.13 Å between Si-O and Al-O increases ΔU by a factor of ten leading to $\Delta U = 0.004$ Å^2. Exactly the same value is calculated from oxygen and T displacement parameters of Oman kinoshitalite refined in space group *C*2/*m* also confirming a disordered model.

Thus, the new data rule out *C*2 or $C\bar{1}$ symmetry combined with twinning as a cause of the observation of average *C*2/*m* diffraction symmetry. Instead, two different disorder models must be considered: (1) three-dimensional Si, Al disorder and (2) one-dimensional disorder along the *c* axis. If one-dimensional disorder is present, individual tetrahedral sheets are completely Si, Al ordered (as in the *C*2 and $C\bar{1}$ model) but there is no ordering relative to the adjacent sheets above or below. Type (1) and type (2) disorder could theoretically be distinguished by ^{29}Si magic angle spinning NMR spectroscopy resolving the local neighborhood of adjacent tetrahedra within one layer. However, in case of natural kinoshitalite such an approach must be abandoned because the occurrence of close to end-member kinoshitalite in nature is so far restricted to Mn-rich rocks, and Mn is also incorporated into the octahedral layers. Even very low concentrations of paramagnetic elements (Fe or Mn in this case) strongly disturb an NMR spectrum (Kirckpatrick 1988). Disordered stacking of completely ordered layers, in terms of stacking faults, should also lead, at least theoretically, to diffuse scattering parallel to the *c* axis. However, in case of kinoshitalite the diffraction pattern is governed by the strong scattering of Ba

and the octahedral sheet. Thus the weak differences between disordered layers with identical topology is not sufficient to cause significant diffuse scattering to be resolved by an X-ray experiment. However, as shown below, there are strong crystal chemical arguments for the presence of stacking faults of completely Si, Al ordered tetrahedral layers.

Ba displacement as an indicator of Si, Al ordering

The tetrahedral layers are rather stiff by condensation in two dimensions and also fixed by an adjacent octahedral sheet. If within such a stiff sheet Si, Al disorder would occur we must expect units of two adjacent Al and two adjacent Si tetrahedra where the former would also violate the Loewenstein (1954) avoidance rule. To balance underbonding, the oxygen atom between two adjacent Al tetrahedra would strongly attract the Ba atom surrounded by a six-membered tetrahedral ring above and below. In contrast, two adjacent Si tetrahedra in such a six-membered ring would repel Ba, leading to strong positional disorder of Ba.

Armbruster (1999) found for armenite, $BaCa_2Al_6Si_9O_{30}\cdot 2H_2O$ where Ba is also capped by two six-membered rings of tetrahedra, that the Ba-O distance to an oxygen connecting two Si tetrahedra is ca 3.2 Å, whereas the distance to an oxygen connecting an Si and an Al tetrahedron is 2.8–2.9 Å. A similar disorder effect should be visible in kinoshitalite if we assume that the oxygen neighbored by two Al tetrahedra shares two Ba sites in adjacent six-membered rings (there is only one Ba bonded to the Si and Al linking oxygen in armenite). This should lead to strong smearing of Ba, in particular within (001), which was not observed in kinoshitalite. The atomic displacement parameters of Ba in kinoshitalite are rather isotropic and the corresponding isotropic equivalent value [B_{eq} = 1.521(4) Å^2] is not much different to the corresponding B_{eq} value of 1.165(6) Å^2 found for armenite with an ordered Si, Al arrangement. Note that a six-membered ring of $Si_4Al_2O_{18}$ composition in armenite is smaller than a $Si_3Al_3O_{18}$ ring in kinoshitalite which also reduces Ba displacement. For a six-membered ring with disordered Si, Al distribution, violating the Al avoidance rule, one would rather expect Ba displacement parameters which are at least increased by a factor of two. Winter et al. (1995) found in a synthetic double-ring silicate a B_{eq} value of 1.847(6) Å^2 for Ba coordinated by two six-membered rings of $Si_4Al_2O_{18}$ composition, though with disordered Si, Al distribution. However, six-membered rings of $Si_4Al_2O_{18}$ composition do not require violation of the Loewenstein (1954) rule thus the Ba disorder is less than expected for three-dimensional Si, Al disorder in kinoshitalite. In anandite-2*O*, with the simplified composition $Ba(Fe^{2+})_3(Si_{2.6}Fe^{3+}_{1.4})O_{10}(OH)S$, Ba is coordinated by two six-membered rings of $Fe^{3+}_{2.8}Si_{3.2}O_{18}$ and $Si_{4.6}Fe^{3+}_{1.4}O_{18}$, respectively, where the former ring has two pairs of adjacent tetrahedra with $Fe^{3+}_{0.7}Si_{0.3}$ occupancy and the latter ring has two pairs of adjacent SiO_4 tetrahedra (Filut et al. 1985). The Ba-O distances vary between 2.97 and 3.27 Å with the shortest Ba-O distances between Ba and the oxygen position linking the two Fe^{3+}-rich tetrahedra. As expected, the longest Ba-O distances are found to oxygen linking two Si tetrahedra. This partially ordered tetrahedral Fe^{3+}, Si distribution in anandite led to a B_{eq} value of 2.04 Å^2 for Ba (Filut et al. 1985), still considerably larger than the Ba displacement in kinoshitalite.

In case of preiswerkite, $Na(Mg_2Al)(Si_2Al_2)O_{10}(OH)_2$, the 1*M* polytype also revealed *C*2/*m* space group symmetry leading to Si, Al disorder, although various spectroscopic methods indicated alternating Al and Si tetrahedra (Oberti et al. 1993). We may therefore suggest that similar stacking faults of completely Si, Al ordered sheets exist in preiswerkite and kinoshitalite where they are responsible for average *C*2/*m* symmetry.

The OH group

The hydrogen of the O4 hydroxyl group in kinoshitalite undergoes a very weak trifurcated hydrogen bond to 2 × O2 (2.74(3) Å) and 1 × O1 (2.81(6) Å). Thus the hydrogen position and bonding scheme is very similar to the one determined for phlogopite and biotite (e.g., Brigatti and Davoli 1990). Oberti et al. (1993) argue that such long H…O distances indicate that the hydrogen bond is not essential for the stability of the mica structure and OH may be substituted by F which is also confirmed by the electron microprobe analyses of kinoshitalite. In contrast, preiswerkite (Oberti et al. 1993) without F substitution has considerably shorter O…H distances of 2 × 2.4 and 1 × 2.5–2.6 Å.

Acknowledgments

Mohammed Bin Hussein Bin Kassim, Director General, and Hilal al Azry, Director Geological Surveys of the Ministry of Petroleum and Minerals of Oman are thanked for organizing necessary permits. Microprobe analyses were supported through Swiss National Sciene Foundation grant 21-26579.89.

References cited

Allemann, F. and Peters, T. (1972) The ophiolite-radiolarite belt of the North-Oman Mountains. Eclogae geologicae Helveticae, 65, 657–697.

Armbruster, T. (1999) Si, Al ordering in the double-ring silicate armentite, $BaCa_2Al_6Si_9O_{30}\cdot 2H_2O$: A single-crystal X-ray and ^{29}Si MAS NMR study. American Mineralogist, 84, 92–101.

Bailey, S.W. (1984) Crystal chemistry of true micas. Mineralogical Society of America Reviews in Mineralogy, 13, 13–60.

Bigi, S., Brigatti, M.F., Mazzucchelli, M., and Rivalenti, G. (1993) Crystal chemical variations in Ba-rich biotites from gabbroic rocks of lower crust Ivrea zone, NW Italy. Contributions to Mineralogy and Petrology, 113, 87–99.

Bloss, F.D., Shekarchi, E., and Shell, H.R. (1959) Hardness of synthetic and natural micas. American Mineralogist, 44, 33–48.

Bol, L.C.G.M., Bos, A., Sauter, P.C.C., and Jansen, J.B.H. (1989) Barium-titanium-rich phlogopites in marbles from Rogaland, southwest Norway. American Mineralogist, 74, 439–447.

Brigatti, M.F. and Davoli, P. (1990) Crystal-structure refinements of 1*M* plutonic biotites. American Mineralogist, 75, 305–313.

Brigatti, M.F. and Poppi, L. (1993) Crystal chemistry of Ba-rich trioctahedral micas-1*M*. European Journal of Mineralogy, 5, 857–871.

Bucher-Nurminen, K. (1982) Mechanism of mineral reactions inferred from textures of impure dolomitic marbles from East Greenland. Journal of Petrology, 23, 325–343.

Chabu, M. and Baulège, J. (1992) Barium feldspar and muscovite from Kingushi Zn-Pb-Cu deposit, Shaba, Zaire. Canadian Mineralogist, 30, 1143–1152.

Dasgupta, S., Chakroborti, S., Sengupta, P., Bhattacharya, P.K., and Banerjee, H. (1989) Compositional characteristics of kinoshitalite form the Sausar Group, India. American Mineralogist, 74, 200–202.

Deer, W.A., Howie, R.A., and Zussmann, J. (1982) Orthosilicates, 2nd edition. Longmans, London.

Edgar, A.D. (1992) Barium-rich phlogopite and biotite from some Quaternary alkali mafic lavas, West Eifel, Germany. European Journal of Mineralogy, 4, 321–330.

Enraf-Nonius (1983) Structure determination package (SDP). Enraf-Nonius, Delft, The Netherlands.

Filut, M.A., Rule, A.C., and Bailey, S.W. (1985) Crystal structure refinement of anandite-2Or, a barium-and sulphur-bearing trioctahedral mica. American Mineralogist, 70, 1298–1308.

Fleischer, M., Chao, G.Y., and Kato, A. (1975) New mineral names. American Mineralogist, 60, 485–489.

Frimmel, H.E., Hoffmann, D., Watkins, R.T., and Moore, J.M. (1995) An Fe analogue of kinoshitalite from the Broken Hill massive sulfide deposit in the Namaqualand Metamorphic Complex, South Africa. American Mineralogist, 80, 833–840.

Frondel, C. and Ito, J. (1967) Barium-rich phlogopite from Långban, Sweden. Arkiv för Mineralogi och Geologi, 4, 445–447.

Gaspar, J.C. and Wyllie, P.J. (1982) Barium phlogopite from the Jacupiranga carbonatite, Brazil. American Mineralogist, 67, 997–1000.

Giuseppetti, G. and Tadini, C. (1972) The crystal structure of 2O brittle mica; anandite. Tschermak's Mineralogische und Petrographische Mitteilungen, 18, 169–184.

Glassley, W.E. (1975) High grade regional metamorphism of some carbonate bodies: significance for the orthopyroxene isograd. American Journal of Science, 275, 1133–1163.

Glennie, K.W., Boeuf, M.G.A., Hughes-Clarke, M.W., Moody-Stuart, M., Pilaar, W.F.H., and Reinhardt, B.M. (1974) Geology of the Oman Mountains. Verhandelingen van het Koninklijk Nederlands Geologisch Mijnbouwkundig Genootschap, 31, 1–423.

Gnos, E. and Kurz, D. (1994) Sapphirine-quartz and sapphirine-corundum assemblages in metamorphic rocks associated with the Semail Ophiolite (United Arab Emirates). Contributions to Mineralogy and Petrology, 116, 398–410.

Gnos, E. and Nicolas, A. (1996) Structural evolution of the northern end of the Oman Ophiolite. Tectonophysics, 254, 111–137.

Gnos, E. and Peters, T. (1995) Tephroite-hausmannite-galaxite from a granulite-facies manganese rock of the United Arab Emirates. Contributions to Mineralogy and Petrology, 120, 372–377.

Gnos, E., Armbruster, T., and Nyfeler, D. (1996) Kanoite, donpeacorite and tirodite: Mn-Mg-silicates from a manganiferous quartzite in the United Arab Emirates. European Journal of Mineralogy, 8, 251–261.

Guggenheim, S. (1984) The brittle micas. Mineralogical Society of America.Reviews in Mineralogy, 13, 61–104.

Guggenheim, S. and Kato, T. (1984) Kinoshitalite and Mn phlogopites: Trial refinements in subgroup symmetry and further refinement in ideal symmetry. Mineralogical Journal, 12, 1–5.

Harlow, G.E. (1995) Crystal chemistry of barian enrichment in micas from metasomatized inclusions in serpentinite, Montagua Fault Zone, Guatemala. European Journal of Mineralogy, 7, 775–789.

Hatch, R., Humphrey, R.A., Eitel, W., and Comerford, J.E. (1957) Synthetic mica investigations IX: reviews of progress from 1947 to 1955. U.S. Department of Interior, Bureau of mines, Investigation Report 5337.

Kato, T., Miúra, Y., Yoshii, M., and Maeda, K. (1979) The crystal structures of 1*M*-kinoshitalite, a new barium brittle mica and the1*M*-manganese trioctahedral micas. Mineralogical Journal, 9, 392–408.

Kickmaier, W. and Peters, T. (1991) Chert-hosted manganese deposits in the Wahrah Formation: A depositional model. In T. Peters, A. Nicolas, and R.G. Coleman, Eds. Ophiolite genesis and evolution of oceanic lithosphere. Proceedings of the Ophiolite Conference, held in Muscat, Oman 1990, 5, p. 647–674. Kluwer Academic Publishers, Dordrecht.

Kirckpatrick, R.J. (1988) MAS NMR spectroscopy of minerals and glasses. In Mineralogical Society of America Reviews in Mineralogy, 18, 341–403.

Kretz, R. (1980) Occurrence, mineral chemistry and metamorphism of Precambrian carbonate rock in a portion of the Grenville Province. Journal of Petrology, 21, 573–620.

Kunz, M. and Armbruster, T. (1990) Difference displacement parameters in alkali feldspars; effects of (Si,Al) order-disorder. American Mineralogist, 75, 141–149.

Loewenstein, W. (1954) The distribution of aluminium in the tetrahedra of silicates and aluminates. American Mineralogist, 39, 92–96.

Lovering, J.F. and Widdowson, J.R. (1968) Electron microprobe analysis of anandite. Mineralogical Magazine, 36, 871–874.

Mansker, W.L., Ewing, R.C., and Keil, K. (1979) Barian-titanian biotites in nephelinites from Oahu, Hawaii. American Mineralogist, 64, 156–159.

Matsubara, S., Kato, A., Nagashima, A., and Matsuo, G. (1976) The occurrence of kinoshitalite from Hokkejino, Kyoto Prefecture, Japan. Bulletin of the Natural Science Museum Series C, 2, 71–78.

Oberti, R., Ungaretti, L., Tilli, A., Smith, D.C., and Robert J.-L. (1993) The crystal structure of preiswerkite. American Mineralogist, 78, 1290–1298.

Pan, Y. and Fleet, M.E. (1991) Barium feldspar and barian-chromian muscovite from the Hemlo area, Ontario. Canadian Mineralogist, 29, 481–498.

Pattiaratchi, D.B., Saari, E., and Sahama, T.G. (1967) Anandite, a new barium iron silicate from Wilagedera, North Western Province, Ceylon. Mineralogical Magazine, 36, 1–4.

Reinhardt, B.M. (1969) On the genesis and emplacement of ophiolites in the Oman Mountains geosyncline. Schweizerische Mineralogische und Petrographische Mitteilungen, 49, 1–30.

Rice, J.M. (1977) Progressive metamorphism of impure dolomitic limestone in the Marysville aureole, Montana. American Journal of Science, 277, 1–24.

Sheldrick, G.M. (1997) SHELX-97, program for crystal structure determination. University of Göttingen, Germany.

Solie, D.N. and Su, S.-C. (1987) An occurrence of Ba-rich micas from theAlaska range. American Mineralogist, 72, 995–999.

Thompson, R.N. (1977) Primary basalts and magma genesis. III Alban Hills, Roman comagmatic province, Central Italy. Contributions to Mineralogy and Petrology, 60, 91–108.

Tracy, R.J. (1991) Ba-rich micas from the Franklin marble, Lime Crest and Sterling Hill, New Jersey. American Mineralogist, 76, 1683–1693.

Wendlandt, R.F. (1977) Barium-phlogopite from the Jaystack Butte, Highwood Mountains, Montana. Carnegie Institution Washington, Year Book, 76, 534–539.

Winter, W., Armbruster, T., and Lengauer, C. (1995) Crystal structure refinement of synthetic osumilite-type phases: $BaMg_2Al_6Si_9O_{30}$, $SrMg_2Al_6Si_9O_{30}$ and $Mg_2Al_4Si_{11}O_{30}$. European Journal of Mineralogy, 7, 277–286.

Yoshii, M. and Maeda, K. (1975) Relations between barium content and the physical and optical properties in the manganoan phlogopite-kinoshitalite series. Mineralogical Journal, 8, 58–65.

Yoshii, M., Maeda, K., Kato, T., Watanabe, T., Yui, S., Kato, A., and Nagashima, K. (1973a) Kinoshitalite, a new mineral from the Noda-Tamagawamine, Iwate Prefecture. Chigaku Kenkyu, 24, 181–190.

Yoshii, M., Togashi, Y., and Maeda, K. (1973b) On the intensity changes of basal reflections with relation to barium content in manganoan phlogopites and kinoshitalite. Bulletin of the Geological Survey of Japan, 24, 1–8.

Zhang, M., Suddaby, P., Thompson, R.N., and Dungan, M.A. (1993) Barian titanian phlogopite from potassic lavas in northwest China: chemistry, substitutions and paragenesis. American Mineralogist, 78, 1056–1065.

MANUSCRIPT RECEIVED JANUARY 25, 1999
MANUSCRIPT ACCEPTED AUGUST 19, 1999
PAPER HANDLED BY LEE A. GROAT